Numerical Analysis of Joint Temperature Evolution During Friction Stir Welding Based on Sticking Contact

Wenya Li, Zhihan Zhang, Jinglong Li, and Y.J. Chao

A three-dimensional numerical model for friction stir welding was developed by using the ABAQUS software based on a fully sticking friction. The temperature measurement was performed to validate the reliability of the model. The simulated thermal histories are in good agreement with the experiments. Simulated results show that the rotation speed has no influence on the time to reach the peak temperature in the workpiece, while the welding speed has significant effect on the time to reach the peak temperature at points away from the plunging center. The value of this peak temperature also changes somewhat. Moreover, the peak temperature in the workpiece tends to reach a quasi-steady state at the beginning of the moving stage; but the temperature at some distance away from the weld does not reach the quasi-steady state during the welding.

1. Introduction

Friction stir welding (FSW), as an innovative solid-state joining process, has received increasing attention in many industrial fields for joining light metallic structures such as aluminum and magnesium alloys. It is known that the microstructure and properties of FSW joints are directly dependent on the temperature during welding. If excessive heat is generated during FSW, the precipitates in the base metal could be dissolved (Ref 1), meanwhile, the nugget zone could be seriously softened as well as the heat-affected zone (HAZ) (Ref 2). Previous research (Ref 3-6) has found that the microhardness profile across the weld region was a "W" or "U" shape. This demonstrates that the joint has been seriously softened owing to the dissolving of many precipitates in the base metal. Therefore, a detailed investigation on the temperature field during FSW is indispensable to the control of joint quality. However, it would be extremely laborious or impossible to explain the underlying nature of the process only by experiments due to the thermo-mechanical coupling. As such, numerous efforts have been dedicated to model the FSW process. Models considering sliding friction have been developed by Chao et al. (Ref 7) and Song et al. (Ref 8). In the latter, the heat input from the tool pin and shoulder was modeled as a moving heat source, and a moving coordinate was used to simplify the moving tool. Moreover, a sticking-sliding model

was proposed by Schmidt et al. (Ref 9, 10) and Maalekian et al. (Ref 11), while other authors have considered only sticking contact (Ref 12-19). There are also other models based on different formulations and assumptions for the temperature field (Ref 20-22).

Up to now, however, it is still being debated whether heat is mainly generated by coulomb or similar friction mechanisms at the tool/workpiece interface (sliding boundary), by plastic deformation in the shear layer (sticking boundary) or by a combination of both. Similarly, the shoulder heat input in all heat resource models were applied as surface heat flux rather than a body heat flux (BHF). In the present work, a three-dimensional (3D) numerical model for the complete FSW process was developed by using the redevelopment technique in the ABAQUS software based on a fully sticking contact to further investigate the heat generation in the FSW process. The heat input was applied to the prescribed shear layer as a BHF, which will be discussed in detail in "Computational Model" section. The effects of the rotation speed of the tool and welding speed on the temperature evolution were discussed.

2. Material and Experimental Procedures

To validate the reliability of the model, FSW experiments were performed on 3.175 mm thick 2024-T3 aluminum alloy sheets at a rotation speed of 300 rpm and a welding speed of 60 mm min^{-1} which were also used in the simulation. The sheets were machined into samples of 200 mm in length by 95 mm in width, and butt-welded parallel to the rolling direction using a CNC milling machine (XKA5032, Nangtong Machine Co. Ltd., China).

The temperature difference between the advancing and retreating sides was found to be small and nonsignificant (Ref 14, 23, 24). In addition, in many publications (Ref 7, 8, 11, 12, 15, 25) the thermal profile was assumed to be symmetric to simplify the temperature measurement and numerical modeling. Considering all these reasons, only one side (retreating side) of

Wenya Li, Zhihan Zhang, and Jinglong Li, State Key Laboratory of Solidification Processing, Shaanxi Key Laboratory of Friction Welding Technologies, Northwestern Polytechnical University, Xi'an 710072 Shaanxi, People's Republic of China; and **Y.J. Chao,** Department of Mechanical Engineering, University of South Carolina, Columbia, SC 29208. Contact e-mail: liwy@nwpu.edu.cn.
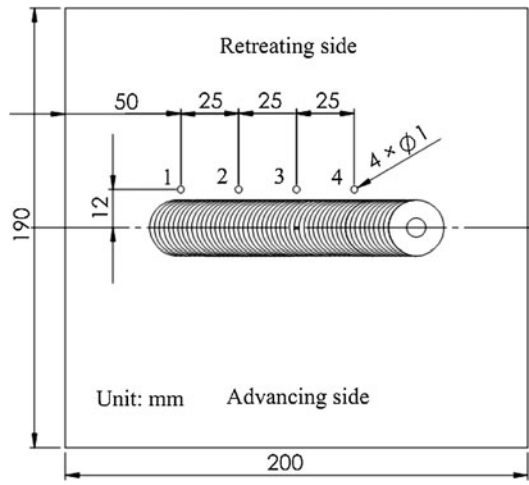
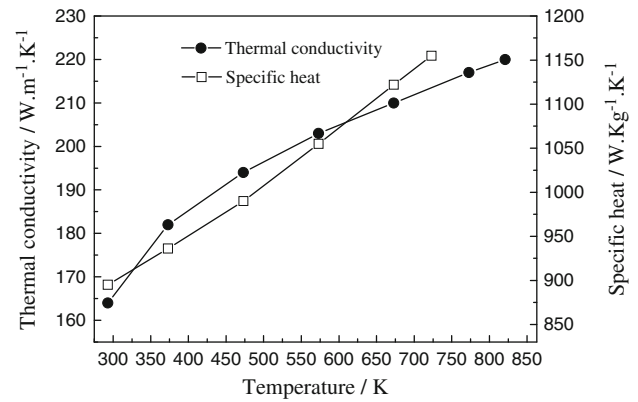Fig. 1 Arrangement of thermocouples at retreating side of the workpiece

Fig. 2 The temperature-dependent conductivity and specific heat of Al2024-T3 (Ref 28)

Table 1 Material constants used in Eq 5 for Al2024-T3 (Ref 27)

A, MPa	B, MPa	T_{ref}, °C	n	C	$\dot{\varepsilon}_0$, s^{-1}
369	684	25	0.73	0.0083	1

the workpiece was chosen for the temperature measurement and modeling. Blind holes having 1 mm diameter and 2 mm depth were drilled for embedding the K-type thermocouples with an outer diameter of 1 mm as illustrated in Fig. 1. The welding was started at a distance of 50 mm away from the edge. The plunging depth of the tool shoulder was 0.35 mm and the weld length was 100 mm. The plunge, dwell and post-weld air-cooling times were 5.7, 10, and 68 s, respectively. The tool made of 1Cr18Ni9Ti austenitic steel was characterized by a non-threaded probe with a 5 mm diameter and 2.5 mm height as well as non-concave shoulder with a 15 mm diameter.

3. Numerical Solutions

3.1 Computational Model

In this study, it was assumed that the probe/workpiece and shoulder/workpiece interfaces present a fully sticking condition, which means that all heat generated in the whole FSW process was attributed solely to the significant plastic deformation in the shear layer of certain thickness. The sticking condition at the probe/workpiece interface was proposed in the literature (Ref 9, 13, 18). However, the results obtained in all publications have been insufficient to determine the condition at the shoulder/workpiece interface up to now. It was also hypothesized that the power of heat generation in the shear layer (P_w) during FSW is equal to the mechanical power associated with the moving tool (P_{tool}):

$$P_w = P_{tool} = M\omega + Fv \qquad \text{(Eq 1)}$$

where M is the torque, ω the rotation speed, F the tool advancing force, and v the welding speed. Cui et al. (Ref 26) found that the term associated with the tool force in Eq 1 was normally less than 1% of P_{tool} and could be ignored for estimating the total tool power. Hence, P_w can be further expressed as:

$$P_w \approx M\omega \qquad \text{(Eq 2)}$$

Theoretically, in addition, a fully sticking condition can be used to estimate the maximum torque value (Ref 9):

$$M = M_{shoulder} + M_{pin\,surface} + M_{pin\,bottom}$$
$$= \frac{\sqrt{3}}{3} \sigma_s r (s_{shoulder} + s_{pin\,surface} + s_{pin\,bottom}) \qquad \text{(Eq 3)}$$

where σ_s is the yield stress, r the distance from the calculated point to the rotating axis, and s the surface area.

The BHF in the shear layer can be obtained from Eq 1-3:

$$BHF = \frac{P_w}{V_{shear\,layer}} = \frac{\sqrt{3}}{3\delta} \sigma_s r \omega \qquad \text{(Eq 4)}$$

where $V_{shear\,layer}$ is the volume of the shear layer ($V_{shear\,layer} = (s_{shoulder} + s_{pin\,surface} + s_{pin\,bottom})\delta$), δ the thickness of the shear layer. $\delta = 0.25$ mm was adopted in the simulation according to (Ref 19, 27).

The temperature-dependent conductivity and specific heat of 2024-T3 aluminum alloy were taken from the literature (Ref 28) as shown in Fig. 2. The Johnson-Cook constitutive equation with the modified temperature term was used in the simulation, which accounts for strain hardening, strain rate hardening and thermal softening effects. Hence the yield stress (σ_s) can be expressed as:

$$\sigma_s = (A + B\varepsilon^n)\left[1 + C \ln\left(\frac{\dot{\varepsilon}}{\dot{\varepsilon}_0}\right)\right] \exp[0.00287(T - T_{ref}) $$
$$- 0.000366(T - T_{ref})^{1.5}] \qquad \text{(Eq 5)}$$

where ε, $\dot{\varepsilon}$, and $\dot{\varepsilon}_0$ are the strain, strain rate (s^{-1}), and reference strain rate (s^{-1}), respectively, T_{ref} the reference temperature, A, B, C, and n are material constants as given in Table 1 (Ref 28). A strain rate of 500 s^{-1} was used in the simulation based on the reported values (Ref 18, 27, 29). However, the strain can be calculated by the following equation because the FSW process is similar to the compression process:

$$\varepsilon = \ln^{\frac{\delta}{\delta - vdt}} \qquad \text{(Eq 6)}$$

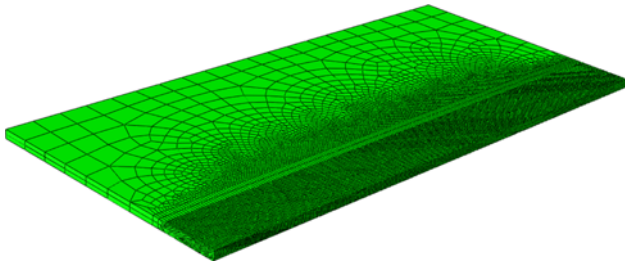where v is the welding speed, dt the time increment within each time step.

Fig. 3 Full view of simulation model and meshing (just one workpiece was used)
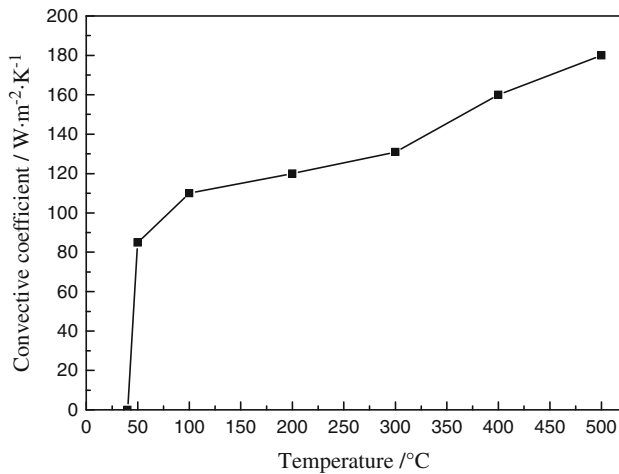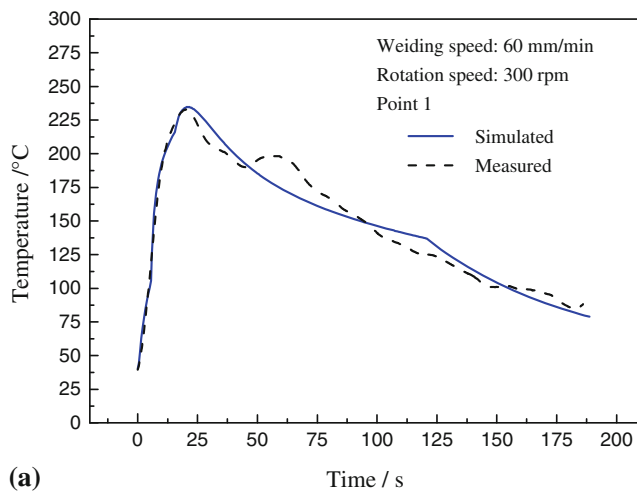

Fig. 4 Change of convective heat transfer coefficient of the bottom surface with temperature

Table 2 The used welding parameters

Tool rotation speed, rpm	300, 400, 500, 600
Welding speed, mm min^{-1}	60, 70, 80, 90

Most of the heat generated at the shear layer will be transported into the workpiece while the rest enters the tool. Theoretically, the fraction of heat transported into the workpiece (f) can be estimated by the following equation based on the thermo-physical properties of the workpiece and tool:

$$f = \frac{\sqrt{\lambda_W \rho_W C_{pW}}}{\sqrt{\lambda_W \rho_W C_{pW}} + \sqrt{\lambda_T \rho_T C_{pT}}} \qquad \text{(Eq 7)}$$

where ρ is the density, C_p the specific heat and λ the thermal conductivity. The subscripts W and T represent the workpiece and tool, respectively. In the present model, f is about 75% according to Eq 7. Hence, according to Eq 4 and 7, the BHF from the tool shoulder can be further expressed as:

$$\text{BHF} = \frac{\sqrt{3}}{3\delta} f \eta \sigma_s r \omega = \frac{\sqrt{3}}{3\delta} f \sigma_s r \omega \qquad \text{(Eq 8)}$$

A non-uniform meshing was used, as shown in Fig. 3, for the workpiece to make a compromise between the computation efficiency and accuracy.

3.2 Boundary Conditions

The heat flux and convection boundary conditions were introduced into the present model. The convection boundary has a convective heat transfer coefficient of 10 W m^{-2} K^{-1} with the ambient temperature of 20 °C for the surfaces exposed to air, which was also used in the literature (Ref 27). At the plunge, dwell, and welding stages, the contact thermal conductivity between the backplate and workpiece was considered as a function of the temperature and pressure. It is understood that the pressure in the workpiece changes in accordance with the tool position. Hence, the contact thermal conductivity can be expressed as the function of the temperature and tool position. In this research, a simplified convective heat transfer coefficient as a function of temperature and position was applied to the bottom surface of workpiece by using the FILM subroutine available in ABAQUS. But at the cooling stage, the convective heat transfer coefficient was only considered as a function of temperature as shown in Fig. 4. Preliminary experiments were conducted to ensure excellent weld surface quality under the selected welding parameters. Hence, the temperatures of the backplate and fixture were a little high, and
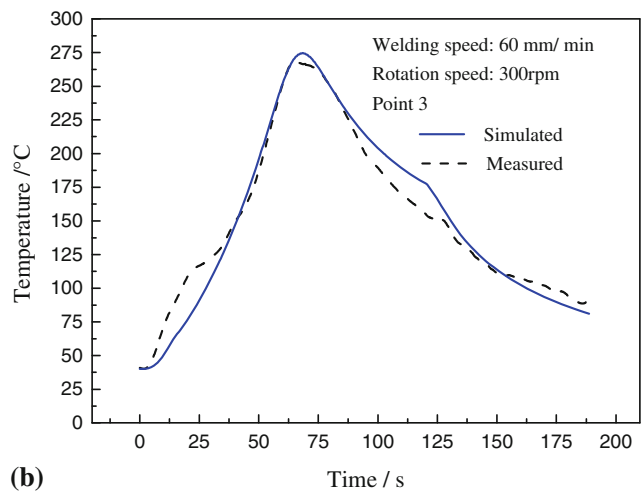
Fig. 5 Comparison of the simulated and experimental temperature curves at points 1 (a) and 3 (b)
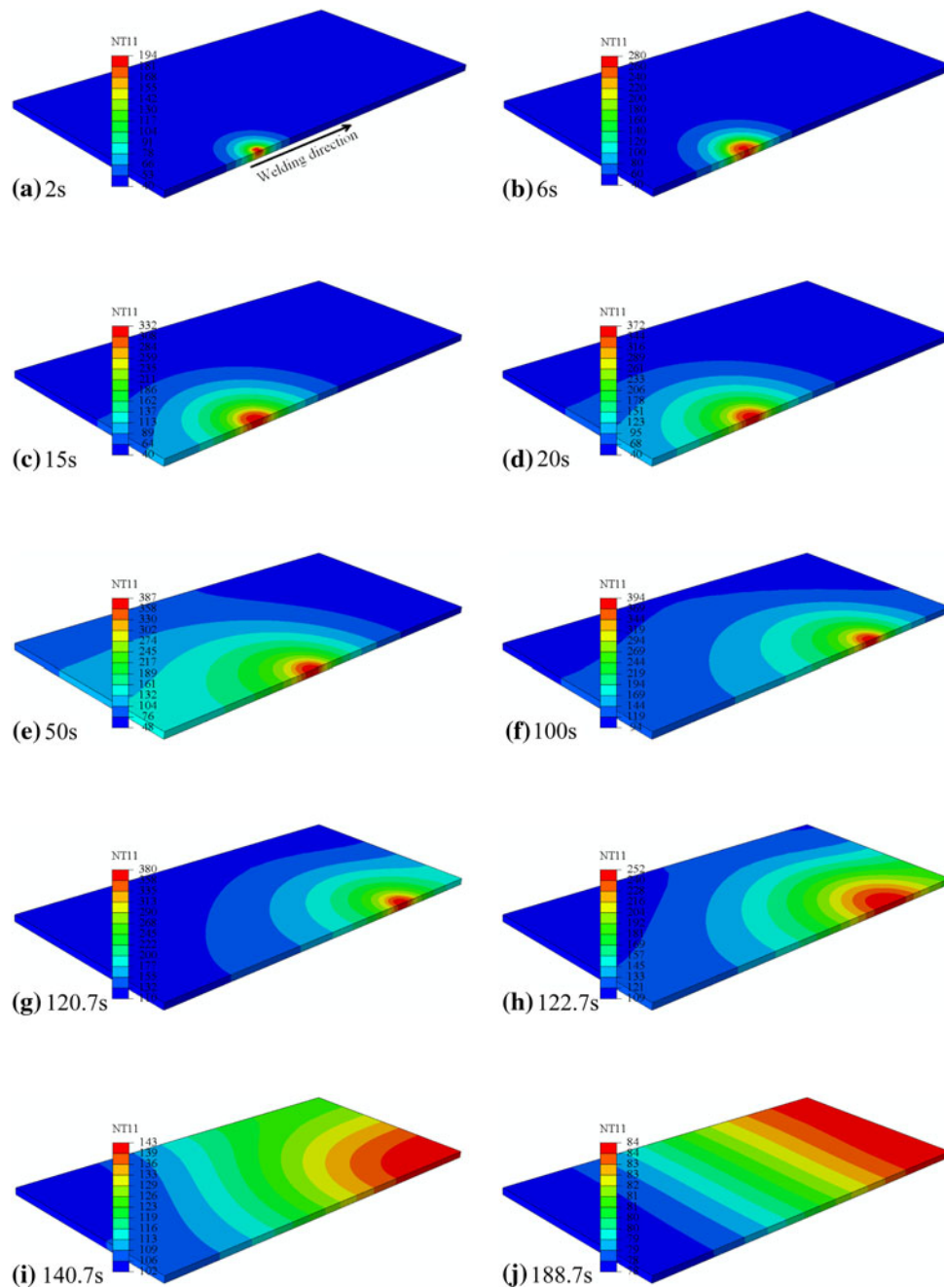
Fig. 6 Temperature contours in the retreating side at different welding times. Note that NT11 means the node temperature

thus the temperature in the measured workpiece was increased to about 40 °C before welding. Therefore, the initial temperature applied to the workpiece in simulations was 40 °C instead of the room temperature. The welding parameters used in the simulation are given in Table 2.

4. Experimental Validation

Figure 5 shows the comparison between the calculated and experimentally recorded temperatures at the points of 1 and 3 (see Fig. 1) at 300 rpm and 60 mm min^{-1}. It can be clearly observed that the changing trends of the calculated temperature curves are in good agreement with the measurements during the entire FSW process, though a little difference in the cooling rate presents, which implies that the cooling rate has been somewhat underestimated by the model. Further study on the contact thermal conductivity between the backplate and workpiece is essential to obtain the actual temperature field. Moreover, when observing the peak temperature, it is interesting to find that it is also comparable to the experiment with a maximum error of about 1.8% only. In addition, it can also be seen that, both the measured and simulated peak temperatures at points 1 and 3 are close to 232 and 270 °C, respectively.
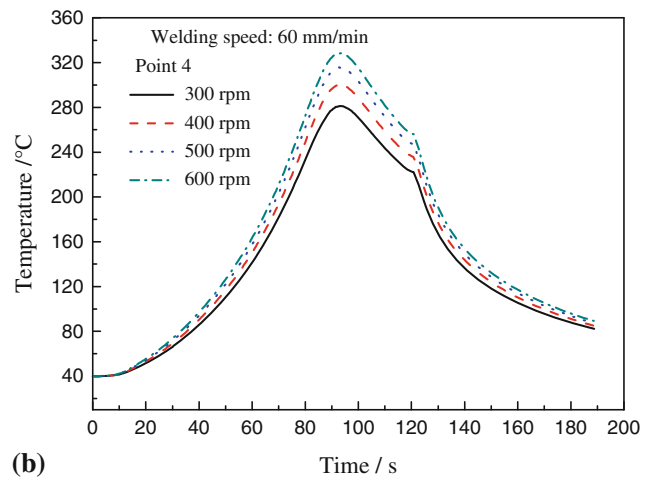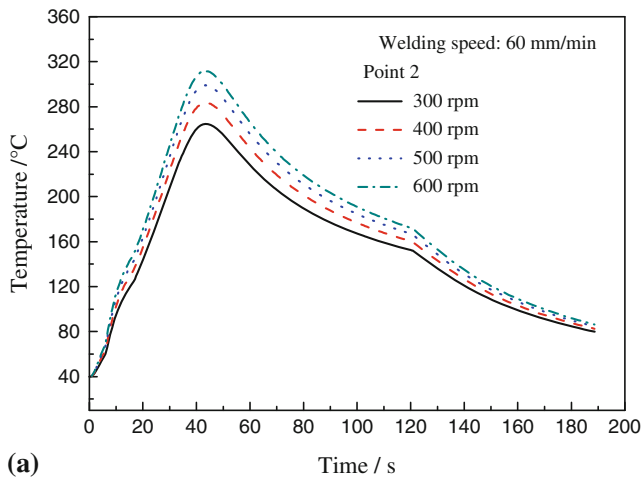
Fig. 7 Effect of rotation speed on the thermal histories of points 2 (a) and 4 (b)

Nevertheless, as expected, the proposed model considering the shear layer appears to be suitable for representing the FSW process.

5. Simulated Results and Discussion

5.1 Representative Temperature Evolution During FSW

Figure 6 shows the transient temperature distribution during the entire FSW process at 300 rpm and 60 mm min^{-1}. As the tool probe plunges, the temperature in the material right under the probe rises quickly to about 194 °C in 2 s (Fig. 6a). It can be seen from Fig. 6(b) that the temperature under the tool shoulder is about 280 °C after contacting with the workpiece. It is noticed from Fig. 6(a)-(c) that the peak temperature presents a sharp increase from about 194 to 332 °C when the welding time is between 2 and 15 s. This temperature increase is because more heat has been produced and conducted into the workpiece after the shoulder contacts with the workpiece. Moreover, with increasing welding time, the high temperature region widens from the probe due to the heat conduction within the workpiece. From Fig. 6(d)-(g), it can be discerned that the peak temperature in the workpiece is about 394 °C during the entire FSW process and it presents a slight variation, which means that a thermal balance between the heat generation and dissipation has formed within and around the stirred zone at this stage and the peak temperature tends to be in a quasi-steady state. When one looks at the cooling stage (see Fig. 6g-j), it is found that the peak temperature decreases sharply from 380 to 252 °C with increasing cooling time from 120.7 to 122.7 s. This means that the fast heat dissipation by heat conduction from the high temperature zone to the cold edges of the workpiece and by the convective heat transfer is relatively large at this stage. However, there is a slight variation in the temperature with increasing cooling time after about 140.7 s.

5.2 Effect of Rotation Speed

To study the effect of rotation speed of the tool on the FSW temperature field, the rotation speed was changed from 300 to 600 rpm with the fixed welding speed of 60 mm min^{-1}.
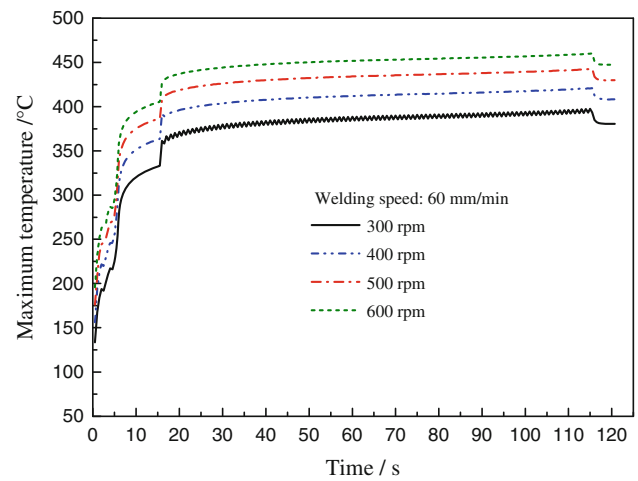

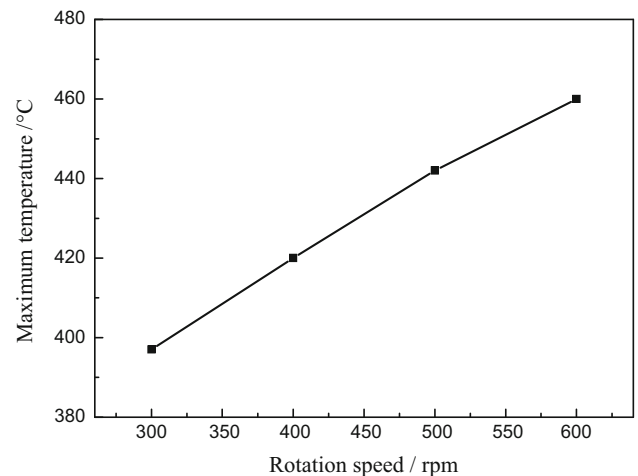**Fig. 8** Temporal variation of the maximum temperature in the whole workpiece

Fig. 9 Effect of rotation speed on the maximum temperature in the whole workpiece
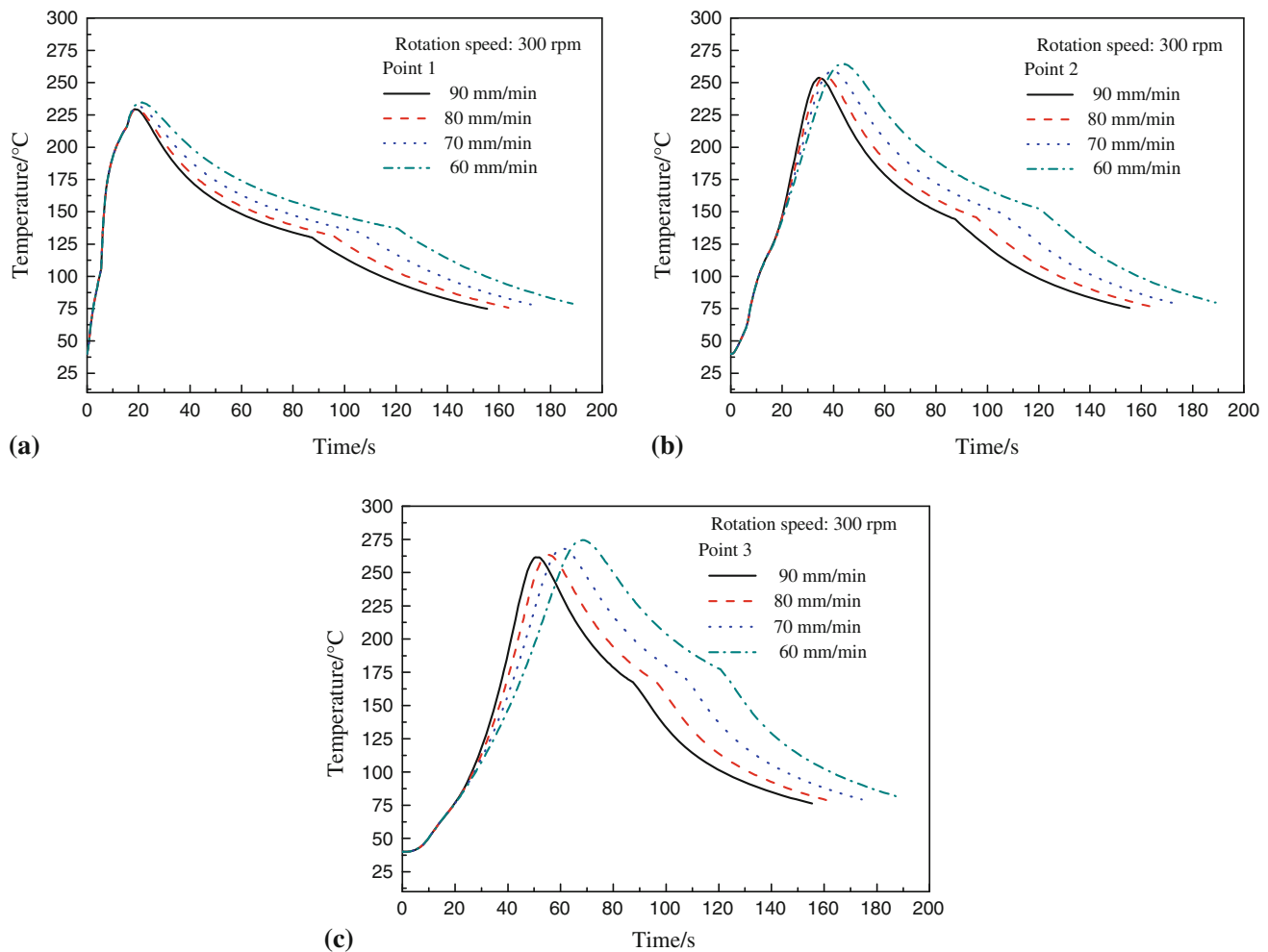
Fig. 10 Effect of welding speed on the thermal histories of points 1 (a), 2 (b), and 3 (c)

Figure 7 shows the effect of rotation speed on the thermal histories of points 2 and 4. It can be seen that each point has experienced a peak temperature under different rotation speeds. Moreover, the times for reaching the peak temperatures at different rotation speeds are almost the same, but the peak values increase with increasing rotation speed. The peak value of point 2 is different from that of point 4 at the same rotation speed, which is consistent with the result in Fig. 5. This means that the temperature at a place far from the weld does not reach a quasi-steady state at the welding stage though the peak temperature in the workpiece has reached a quasi-steady state (see Fig. 6d-g).

Figure 8 shows the evolution of the maximum temperature in the workpiece with the welding time under different rotation speeds. It can be seen that with increasing welding time, the maximum temperature ascends quickly in the early stage and reaches to a temperature plateau at about 18 s. However, the temperature plateau is different under different rotation speeds, and that material at the same position in the workpiece will experience higher temperature at a higher rotation speed.

The effect of the rotation speed on the maximum temperature is shown in Fig. 9 (replot from Fig. 8). It can be found that the temperature increment is about 22 °C when the rotation speed increases from 300 to 400 rpm, and the maximum temperature almost increases linearly with increasing rotation speed from 300 to 600 rpm. According to Eq 8, the BHF also increases linearly with increasing rotation speed. In addition, according to Eq 5, the yield stress decreases exponentially with increasing temperature. Hence, it is reasonable that the maximum temperature almost increases linearly with increasing rotation speed from 300 to 600 rpm due to the slight variation of the yield stress resulting from the increase of the temperature. According to Eq 5 and 8, moreover, the BHF will increase with the augment of rotation speed while the yield stress decreases with the increase of temperature which results from the augment of BHF. This may suggest that the "self-adaptive adjustment" of material mechanical property under the applied thermal and mechanical loads is responsible for this phenomenon. This is also supported by the discussion of the relationship between tool slip and weld temperature (Ref 15).

5.3 Effect of Welding Speed

Figure 10 shows the effect of the welding speed on the temperature evolution at specific points in the workpiece at the rotation speed of 300 rpm. It can be seen from Fig. 10(a) that changing welding speed has little influence on the time for reaching the peak temperature at point 1 in the vicinity of plunging center when the rotation speed is a constant, but the peak temperature decreases slightly with the increase of the

welding speed because of less heat accumulation. However, it can be found from Fig. 10(b) and (c) that with increasing welding speed the times for reaching the peak temperature at points 2 and 3 become shorter and the peak values decrease slightly. According to Eq 5, 6, and 8, with increasing welding speed the BHF will increase when other variables are constant, which means that the peak temperature in the workpiece will increase. This result seems to be inconsistent with the numerical simulation results. The reason for this is that the effect of welding time on the heat accumulation was neglected in above-mentioned analysis.

6. Conclusions

The complete welding process of FSW Al2024-T3 was simulated based on a 3D numerical finite element model. The effects of the rotation and welding speeds on the temperature evolution were systematically discussed. The following conclusions can be drawn:

(1) At the rotation speed of 300 rpm and welding speed of 60 mm min^{-1}, the calculated thermal histories are in agreement with the experiments and the simulated peak temperature in the workpiece is approximately 394 °C during the entire FSW process.

(2) The peak temperature in the workpiece near the weld tends to be in a quasi-steady state at the beginning of the moving stage, but not at a place far from the weld.

(3) Increasing the rotation speed has no influence on the time for reaching the peak temperature in the workpiece at a constant rotation speed, but the peak value gradually increases with the augment of the rotation speed. Moreover, changing welding speed has significant effect on the time for reaching the peak temperature at points away from the plunging center when the welding speed is a constant and the value of this peak temperature also changes somewhat.

References

1. Y. Sato, H. Kokawa, and M. Enomoto, Microstructural Evolution of 6063 Aluminum during Friction Stir Welding, *Metall. Mater. Trans. A*, 2000, **30**, p 2429–2437

2. C.J. Dawes and W.M. Thomas, Friction Stir Process for Aluminum Alloys, *Weld. J.*, 1996, **75**, p 41–45

3. H. Fujii, Y.F. Sun, and H. Kato, Microstructure and Mechanical Properties of Friction Stir Welded Pure Mo Joints, *Scripta Mater.*, 2011, **64**, p 657–660

4. L. Fratini, G. Buffa, and R. Shivpuri, Mechanical and Metallurgical Effects of in Process Cooling during Friction Stir Welding of AA7075-T6 Butt Joints, *Acta Mater.*, 2010, **58**, p 2056–2067

5. H.J. Liu, H.J. Zhang, and L. Yu, Effect of Welding Speed on Microstructures and Mechanical Properties of Underwater Friction Stir Welded 2219 Aluminum Alloy, *Mater. Des.*, 2219, **32**, p 1548–1553

6. M. Peel, A. Steuwer, M. Preuss, and P.J. Withers, Microstructure, Mechanical Properties and Residual Stresses as a Function of Welding Speed in Aluminium AA5083 Friction Stir Welds, *Acta Mater.*, 2003, **51**, p 4791–4801

7. Y. Chao and X. Qi, Thermal and Thermo-Mechanical Modeling of Friction Stir Welding of Aluminum Alloy 6001-T6, *J. Mater. Process. Manuf. Sci.*, 1998, **7**, p 215–233

8. M. Song and R. Kovacevic, Thermal Modeling of Friction Stir Welding in a Moving Coordinate and Its Validation, *Int. J. Mach. Tool Manuf.*, 2003, **43**, p 605–615

9. H. Schmidt, J. Hattel, and J. Wert, An Analytical Model for the Heat Generation in Friction Stir Welding, *Modell. Simul. Mater. Sci. Eng.*, 2004, **12**, p 143–157

10. H. Schmidt and J. Hattel, Thermal Modelling of Friction Stir Welding, *Scripta Mater.*, 2008, **58**, p 332–337

11. M. Maalekian, E. Kozeschnik, H.P. Brantner, and H. Cerjak, Comparative Analysis of Heat Generation in Friction Welding of Steel Bars, *Acta Mater.*, 2008, **56**, p 2843–2855

12. P. Ulysse, Three-Dimensional Modeling of the Friction Stir-Welding Process, *Int. J. Mach. Tool Manuf.*, 2002, **42**, p 1549–1557

13. P.F. Mendez, K.E. Tello, and T.J. Lienert, Scaling of Coupled Heat Transfer and Plastic Deformation around the Pin in Friction Stir Welding, *Acta Mater.*, 2010, **58**, p 6012–6026

14. M.Z.H. Khandkar and J.A. Khan, Thermal Modeling of Overlap Friction Stir Welding for Al-alloys, *J. Mater. Process. Manuf. Sci.*, 2001, **10**, p 91–105

15. M.Z.H. Khandkar, J.A. Khan, and A.P. Reynolds, Prediction of Temperature Distribution and Thermal History during Friction Stir Welding: Input Torque Based Model, *Sci. Technol. Weld. Join.*, 2003, **8**, p 165–174

16. R. Nandan, G.G. Roy, and T. DebRoy, Numerical Simulation of Three-dimensional Heat Transfer and Plastic Flow during Friction Stir Welding, *Metall. Mater. Trans. A*, 2006, **37**, p 1247–1259

17. R. Nandan, G.G. Roy, T.J. Lienert, and T. DebRoy, Numerical Modelling of 3D Plastic Flow and Heat Transfer during Friction Stir Welding of Stainless Steel, *Sci. Technol. Weld. Join.*, 2006, **11**, p 526–537

18. R. Nandan, G.G. Roy, T.J. Lienert, and T. DebRoy, Three-dimensional Heat and Material Flow during Friction Stir Welding of Mild Steel, *Acta Mater.*, 2007, **55**, p 883–895

19. S. Xu, X. Deng, A.P. Reynolds, and T.U. Seidel, Finite Element Simulation of Material Flow in Friction Stir Welding, *Sci. Technol. Weld. Join.*, 2001, **6**(3), p 191–193

20. V. Soundararajan, S. Zekovic, and R. Kovacevic, Thermo-Mechanical Model with Adaptive Boundary Conditions for Friction Stir Welding of Al 6061, *Int. J. Mach. Tool Manuf.*, 2005, **45**, p 1577–1587

21. D. Kim, H. Badarinarayan, J.H. Kim, C. Kim, K. Okamoto, R.H. Wagoner, and K. Chung, Numerical Simulation of Friction Stir Butt Welding Process for AA5083-H18 Sheets, *Eur. J. Mech. A-Solid*, 2010, **29**, p 204–215

22. F. Gemme, Y. Verreman, L. Dubourg, and M. Jahazi, Numerical Analysis of the Dwell Phase in Friction Stir Welding and Comparison with Experimental Data, *Mater. Sci. Eng. A*, 2010, **527**, p 4152–4160

23. W. Tang, X. Guo, J.C. McClure, L.E. Murr, and A. Nunes, Heat Input and Temperature Distribution in Friction Stir Welding, *J. Mater. Process. Manuf. Sci.*, 1998, **7**(2), p 163–172

24. G. Buffa, J. Hua, R. Shivpuri, and L. Fratini, A Continuum Based Fem Model for Friction Stir Welding—Model Development, *Mater. Sci. Eng. A*, 2006, **419**, p 389–396

25. C.M. Chen and R. Kovacevic, Finite Element Modeling of Friction Stir Welding—Thermal and Thermomechanical Analysis, *Int. J. Mach. Tool Manuf.*, 2003, **43**(13), p 1319–1326

26. S. Cui, Z.W. Chen, and J.D. Robson, A Model Relating Tool Torque and Its Associated Power and Specific Energy to Rotation and Forward Speeds during Friction Stir Welding/Processing, *Int. J. Mach. Tool Manuf.*, 2010, **50**, p 1023–1030

27. H. Schmidt, J. Hattel, and J. Wert, A Local Model for the Thermo-Mechanical Conditions in Friction Stir Welding, *Modell. Simul. Mater. Sci. Eng.*, 2005, **13**, p 77–93

28. H.K. Li, Q.Y. Shi, T. Li, and W. Wang, Auto-adaptive Heat Source Model for Numerical Analysis of Friction Stir Welding, *Mater. Sci. Forum*, 2008, **580-582**, p 267–270

29. O.T. Midling and Ø. Grong, A Process Model for Friction Welding of Al-Mg-Si Alloys and Al-SiC Metal Matrix Composites-I. Haz Temperature and Strain Rate Distribution, *Acta Metall. Mater.*, 1994, **42**(5), p 1595–1609